Supporting Information

Controlled and Tunable Loading and Release of Vesicles by Using Gigahertz Acoustics

Yao Lu[+], Wilke C. de Vries[+], Nico J. Overeem[+], Xuexin Duan,* Hongxiang Zhang, Hao Zhang, Wei Pang, Bart Jan Ravoo,* and Jurriaan Huskens*

anie_201810181_sm_miscellaneous_information.pdf
anie_201810181_sm_Video_S1.avi
anie_201810181_sm_Video_S2.avi
anie_201810181_sm_Video_S3.avi
anie_201810181_sm_Video_S4.avi
anie_201810181_sm_Video_S5.avi
anie_201810181_sm_Video_S6.avi
anie_201810181_sm_Video_S7.avi
anie_201810181_sm_Video_S8.avi

Materials and Methods

General: 1,2-Dioleoyl-sn-glycero-3-phosphocholine (DOPC), 1,2-dipalmitoyl-sn-glycero- 3-phosphoethanolamine-N-(cap biotinyl), sodium salt (biotinyl-Cap-PE), and 1-palmitoyl- 2-(dipyrrometheneboron difluoride)undecanoyl-sn-glycero-3-phosphoethanolamine (Top Fluor-PE) were purchased from Avanti Polar Lipids and dissolved in chloroform. Texas Red-modified 1,2-dihexadecanoyl-*sn*-glycero-3-phosphoethanolamine (Texas Red-DHPE), non-fluorescent and Alexa Fluor 488-labeled streptavidin (SAv) were purchased from Thermo Fisher Scientific Inc. Other chemicals were purchased from Sigma Aldrich, VWR or TCI and used without further purification.

4-(2-Hydroxyethyl)piperazine-1-ethanesulfonic acid (HEPES) buffered saline (HBS, 20 mM HEPES, 150 mM NaCl, pH 7.4) was prepared using ultrapure water and used as the buffer solution throughout the work in this chapter. Adamantane-terminated poly(acrylic acid) (Ad-PAA),[1] amphiphilic β-cyclodextrin,[2] rhodamine B labeled amphiphilic β-cyclodextrin,[3] and biotin-NH$_2$[4] were prepared according to previously described procedures. SAv was dissolved in 0.1 M PBS buffer (0.1 M sodium dihydrogen phosphate and 0.15 M sodium chloride, pH 7.4) at a concentration of 20 μg mL^{-1}. Amine-modified polystyrene nanoparticles (PS NPs) (2.5 wt.% in aqueous solution) with different fluorescence markers were purchased from Sigma Aldrich and diluted 10 times with Milli-Q water before use.

Preparation of PSVs: PSVs were prepared according to a previously described method.[4] Briefly, a 2 mM stock solution of amphiphilic β-cyclodextrin in chloroform was added in a round bottom flask and evaporated under a stream of argon to obtain a thin film. Residual solvent was removed under vacuum before the film was hydrated by addition of buffer or carboxyfluorescein (CF) dye solution and stirred for 2 h. The solution was sonicated for 15 s and repetitively passed through a polycarbonate membrane with 100 nm pore size in a Liposofast manual extruder (AVESTIN) to yield cyclodextrin vesicles (CDVs). To stabilize CDVs with a polymer shell, 25 μM Ad-PAA was added to a buffered solution of CDVs (100 μM amphiphilic β-cyclodextrin), and this mixture was gently stirred for 30 min to obtain polymer-decorated vesicles. For crosslinking of the polymer shell, 9 mM 1-ethyl-3-(3-dimethylaminopropyl)carbodiimide hydrochloride (EDC·HCl) was added. After 20 min, 600 μM 2,2'-(ethylenedioxy)bis(ethyleneamine) and optionally, for the biotin-conjugated PSVs, 30

μM biotin-NH$_2$ was added, and the colloid was slowly stirred overnight. Purification of PSVs was performed as described below.

For the release of cargo from PSVs in solution, PSVs were prepared in HBS buffer containing 5 mM CF. Before the release experiment, PSVs were separated from excess CF dye and byproducts by size exclusion chromatography (Sephadex G-50 Superfine) with HBS as the eluent.

For the release of cargo from PSVs immobilized on a surface, PSVs conjugated with biotin-NH$_2$ were prepared in HBS buffer with either 5 mM CF for fluorescence spectroscopy investigations, or with 100 μM CF for fluorescence microscopy measurements. Before the fluorescence spectroscopy investigations, PSVs were separated from excess CF dye and byproducts by size exclusion chromatography with HBS as the eluent. PSVs for fluorescence microscopic experiments were purified by dialysis (Spectra/Por regenerated cellulose (RC) dialysis membranes, MWCO 6–8 kDa, Spectrum Laboratories) against HBS (3 × buffer exchange within 48 h).

Rhodamine B-labelled PSVs conjugated with biotin-NH$_2$ were prepared from CDVs containing 5 mol% rhodamine B-labelled amphiphilic cyclodextrin in HBS buffer. After that PSVs were also purified by dialysis.

For encapsulation of cargo into PSVs immobilized on a surface, PSVs conjugated with biotin-NH$_2$ were prepared in HBS and purified by dialysis.

Dynamic light scattering (DLS): DLS was performed using a Nanotrac instrument (Anaspec), and data were processed with the Microtrac FLEX Operating Software. All the measurements were performed in HBS buffer using 1 mL centrifuge tubes. The average of five measurements was used as the size distribution of PSVs for each experiment.

Transmission electron microscopy (TEM): 5 μL of the PSV sample was incubated on a carbon coated copper grid (glow-discharged in an oxygen plasma) for 2 min and gently blotted with filter paper. The sample was stained with 5 μL of 0.5 % (w/w) aqueous phosphotungstic acid for 1 min and again gently blotted with filter paper. TEM measurements were performed at the Institute of Materials Physics, Münster, Germany, using a Zeiss 200 FE electron microscope with Schottky emitter and energy Ω filter operating at 200 kV. The microscope

was equipped with a CCD camera Gatan USC 4000, and pictures were processed using ImageJ version 1.51n.

Immobilization of PSVs:

Preparation of glass substrates. After sonication in acetone, ethanol and ultrapure water (each for 10 min), the pre-cleaned substrates of cover glass were immersed in a freshly prepared piranha solution (concentrated H_2SO_4/H_2O_2 (30%) = 3/1 (v/v)) for 30 min. Then the substrates were extensively washed with ultrapure water and dried in a stream of nitrogen.

Preparation of PDMS stamps. PDMS stamps were prepared by casting a 10:1 mixture of poly(dimethyl siloxane) and curing agent (Sylgards 184, Dow Corning) on a line-patterned silicon master. The silicon master with 10 μm wide line features separated by 10 μm spacing was fabricated by photolithography. The PDMS mixture was cured at 80 °C overnight. The cured stamp was peeled off from the master at the curing temperature and cut into square pieces.

Patterning PSV by micromolding in capillaries (MIMIC). The patterned PDMS stamp was oxidized in oxygen plasma for 30 s to form hydrophilic interface and quickly placed in contact with the cleaned glass substrate, so that the grooves in PDMS form capillaries between the surface and the stamp. Poly-L-lysine PLL-*g*-OEG-biotin (200 μL, 0.1 mg mL^{-1}, HBS) was pipetted and dropped at the open end of the stamp. The solution spontaneously filled the channels under the capillary pressure. After 20 min, the stamp was gently removed, and the glass substrate was repeatedly washed with HBS (three times). Afterwards, the glass substrate was incubated with streptavidin (200 μL, 30 μg mL^{-1}, HBS) for 15 min and rinsed with HBS again (three times). After that, the pattered glass substrate was incubated with biotinylated PSVs for 5 min and rinsed with HBS (three times) to remove excess biotinylated PSV.

Preparation of the supported lipid bilayer: In this work, lipid mixtures of DOPC, Texas Red-DHPE and Biotinyl-cap-PE (molar ratio is 99.85:0.05:0.1) were used to form the supported lipid bilayer (SLB) using the vesicle fusion method. First, large unilamellar vesicles (LUVs) were prepared using the hydration and extrusion method. In brief, a solution of DOPC (10 mg mL^{-1} in chloroform, 99.85 μL), Texas Red-DHPE (0.2 mg mL^{-1} in methanol, 7.07 μL) and Biotinyl-cap-PE (0.2 mg mL^{-1} in chloroform, 8.78 μL) was injected into a glass vial and

evaporated under a gentle flow of nitrogen gas until the film of lipid was visible on the wall. Then, the vial was put into a vacuum desiccator for more than 1 h to dry the lipids. Thereafter, the dry lipid mixtures were hydrated with 1 mL Milli-Q water and vortexed until all lipids were removed from the vial. The obtained lipid solution was then extruded 11 times using a Mini-Extruder kit (Avanti Polar Lipids) equipped with a polycarbonate membrane of 100 nm pores (Whatman) to form LUVs. In this work, the supported lipid bilayer (SLB) was deposited in the wells of a 96-well-plate with a glass bottom. Before the formation of the SLB, 400 µL sodium hydroxide (NaOH, 1 M) solution was added into the well-plate for 1 h to make the surface hydrophilic. Afterwards, the wells were rinsed with Milli-Q water three times and incubated with 200 µL LUV solution for 30 min at room temperature. A detect-free SLB was then formed by the rupture of LUVs onto the hydrophilic glass substrate. Excess lipids were removed from the well by rinsing with Milli-Q water three times.

Preparation of giant unilamellar vesicles: Two types of giant unilamellar vesicles (GUVs) were prepared using an electrical method. One was composed of DOPC, Texas Red-DHPE and Biotinyl-cap-PE with a molar ratio of 99.85:0.05:0.1. The other one was composed of DOPC, Top Fluor-PE and Biotinyl-cap-PE with a molar ratio of 99.7:0.2:0.1. The mixed lipid solutions were dropped on a titanium oxide-coated glass slide and evaporated with a flow of nitrogen gas to create a uniform lipid film. The lipid-coated slide was dried in a vacuum desiccator for 1 h. Then, the dried lipid-coated slide and a clean non-lipid-coated slide were put together to form a capacitor cell. The conductive sides of both slides were faced inward and were fixed with a clamp to form a chamber. The chamber was filled with 200 mM sucrose (Sigma-Aldrich) solution in Tris buffer (20 mM) and sealed with plastic paraffin film. Electro-formation was then carried out using a function generator. A 10 Hz sinusoidal potential with a 1 V peak-to-peak amplitude was applied across the chamber for 2 h, after which the frequency was reduced to 2 Hz for 1 h. The GUVs were extracted from the chamber using a pipette and stored in a vial (Eppendorf) in the dark.

Immobilization of giant unilamellar vesicles: Before the adhesion of GUVs, the SLB-coated substrate was incubated with SAv/ Alexa Fluor 488 SAv (200 µL, 20 µg mL^{-1}) for 20 min and then rinsed consecutively with PBS and sucrose buffer, each for three

times. After that, 50 μL GUV solutions were added to the well and incubated for another 30 min. Then, the well was gently rinsed with sucrose buffer three times to remove excess GUVs.

NEMS resonator: The resonator was fabricated using standard microfabrication techniques according to a previous published process. A typical sandwiched structure that comprising two molybdenum (Mo) layers as electrodes (top and bottom) and a piezoelectric layer of aluminium nitride (AlN) in the middle was deposited on stacked reflector substrates to generate acoustic streaming in solution. For the NEMS bulk acoustic wave resonator used in this work, the ultra-harmonics were restrained by the Bragg reflector and it is primarily the longitudinal mode that determines its resonance frequency at 2.5 GHz. The resonance frequency was obtained by a network analyzer (Agilent E5061B), from which we calculated that the electromechanical coupling factor (kt^2) of this resonator is 1.6%, which is sufficient for the generation of hypersound.

Chamber-based loading/release system: For studying the loading/release of immobilized PSVs, a square piece of PDMS of 600 μm was punctured with a hole in the center (diameter: 1.5 cm) and sealed on top of the resonator. After filling with HEPES buffered saline (HBS, pH 7.4) (or 5 mM CF dye solution in HBS, 50 μL), a cover glass with immobilized biotinylated PSVs was then placed on top of the chamber, aligning the center of the device. Sinusoidal signals of 2.5 GHz were generated by a signal generator (Mini-Circuits, D500), amplified by a power amplifier (Mini-Circuits, ZHL-5W-422), and sent to the device, which then transduced the electrical supply to mechanical vibrations in solution. The electric input can be conveniently switched on and off using a program control, thus the stimulation time is well controlled.

For PSVs release system in solution, PDMS with thickness of 1.6 cm was cut into square pieces and a hole was punched in the center to form chambers (volume: 150 μL). A chamber was first sealed on top of the resonator and filled with CF-encapsulated PSVs, then a dialysis membrane (MWCO 12–15 kDa, Spectrum Laboratories) was covered on top the chamber, followed by overlay of another chamber with the same size. Before

applying the acoustic stimulation, the upper chamber was filled with HBS buffer, which was then taken out for fluorescence measurements.

Dialysis experiments: For cargo release from PSVs in solution, fluorescence spectra of CF were measured immediately or upon waiting for 20 and 40 min after the acoustic stimulation was turned off to ensure that the released CF dye in the lower chamber can pass through the filter membrane and equilibrate before fluorescence quantification. As shown in Figure. S6, the fluorescence intensity detected at 20 min is higher than right after applying stimulation, while the peak intensity at 40 min is similar to that at 20 min, indicating that the released CF dye has reached equilibrium within 20 min after stimulation is turned off. Therefore, all other measurements were done while waiting for 20 min after ending the stimulation.

Fluorescence spectrometer: The emission spectra of CF (excitation at $\lambda = 488$ nm) and Rhodamine B (excitation at $\lambda = 550$ nm) were recorded using a fluorescence spectrometer (Perkin Elmer). For control experiments, HBS buffer in the upper PDMS chamber was detected without applying hypersound in the lower chamber, however, the fluorescence measurement still started after 20 min to keep in accordance with the conditions of hypersound-trigged experiments.

Fluorescence microscopy: Fluorescent micrographs of PSVs were taken using an inverted research microscope (Olympus, IX71) equipped with a mercury burner (U-RFL-T) as a light source and a digital camera (Olympus, DP70) for image acquisition. Green excitation light (510 nm $\leq \lambda \leq$ 550 nm) and red emission light ($\lambda > 590$ nm) was filtered using a filter cube (U-MWG Olympus). To avoid the photo-bleaching of CF, new areas were selected after each shot. The focusing time before taking the micrographs was 20 s and the magnification times is 10 in all cases.

Confocal laser scanning microscopy (CLSM, Nikon A1) were used to observe immobilized GUVs and the SLB. The Texas Red-labeled GUVs were examined by CLSM and fluorescence microscopy with an excitation wavelength (λ_{ex}) of 595 nm, while the Top Fluor-labeled GUVs were measured with λ_{ex} of 495 nm.

Additional Experimental Data

1. Controlled loading by and release from PSVs

For the loading experiments, as the control group ("no stimulation") in Figure S1a-d shows, PSVs that were incubated with CF dye for 15 min and then rinsed with HBS buffer for three times showed no green florescence in the absence of hypersound, suggesting that there is no interaction between the PSVs and the CF dye. In contrast, application of hypersound does lead to an increase of the fluorescence intensities, as shown in Figure S1a-d. Thus, the occurrence of green fluorescence within the patterned areas is attributed to the loading of CF upon the stimulation by hypersound.

The loading data shown in Figure 1d was fitted linearly, as shown in Figure S1e. The slopes of these fits, called loading rates, were plotted vs power, as shown in Figure S1f. The trend shows that the loading rate is linearly dependent on the power of the acoustic streaming.
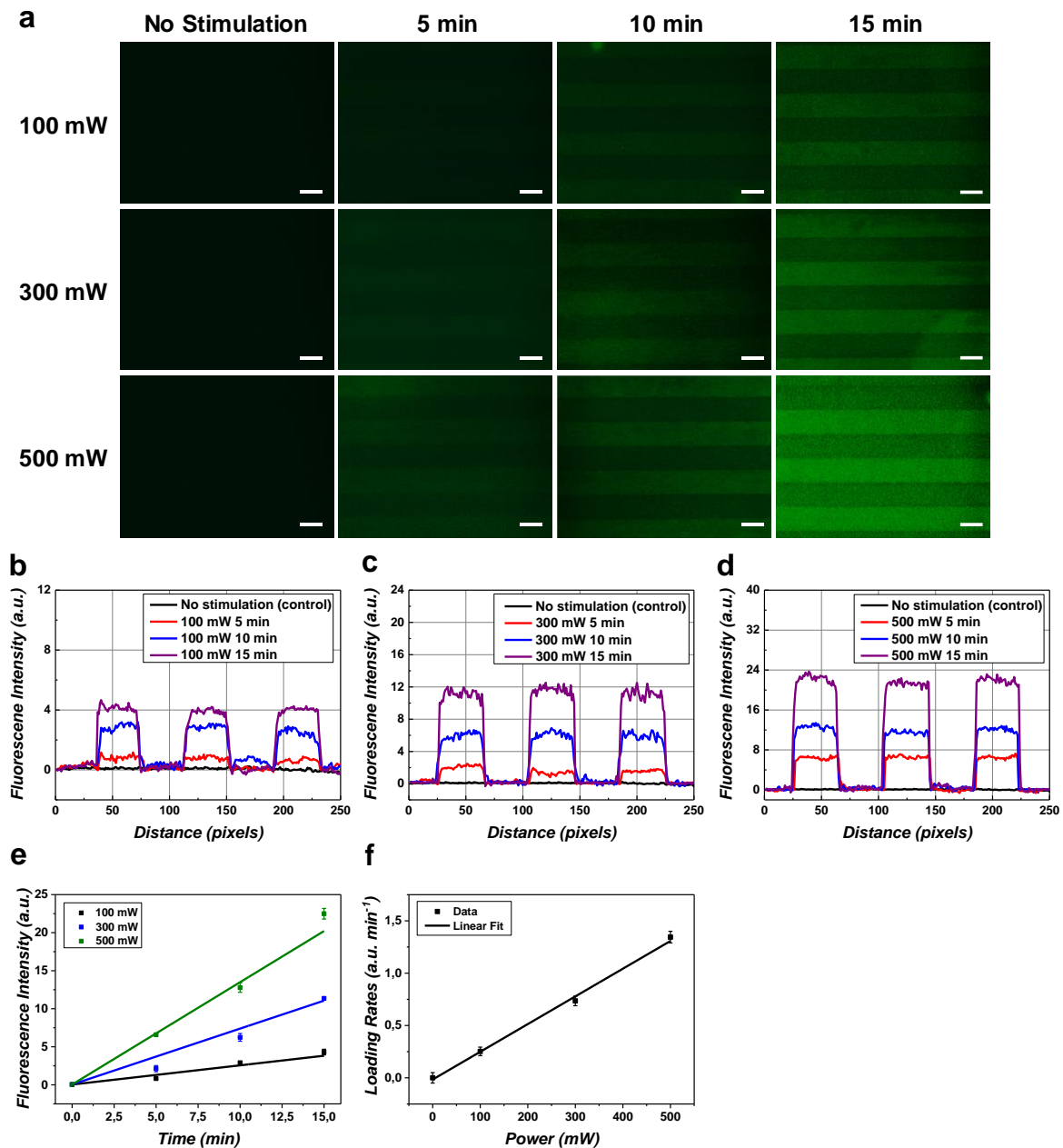
Figure S1. (a) Fluorescence imaging of line-patterned (by MIMIC), immobilized PSVs after loading with CF under acoustic stimulation at different powers (100, 300 and 500 mW) and durations (5, 10 and 15 min). The scale bars indicate 10 μm. Line profiles of fluorescence intensity under acoustic stimulation at (b) 100, (c) 300 and (d) 500 mW. (e) The fluorescence intensities of the loaded CF dye as a function of time at different powers, and linear fits to this data. The fluorescence intensity at 0 min was obtained by measuring the PSVs that were incubated in 5 mM CF solutions for 15 min. (f) Loading rates as a function of power and a linear fit to it.

For the release of CF dye from immobilized PSVs, the intensity-decrease curve were fitted by an exponential decay function (Figure S2e), the time constant of which was extracted and used as the release rate. In Figure S2f, the release rates demonstrate a linear trend at different powers.
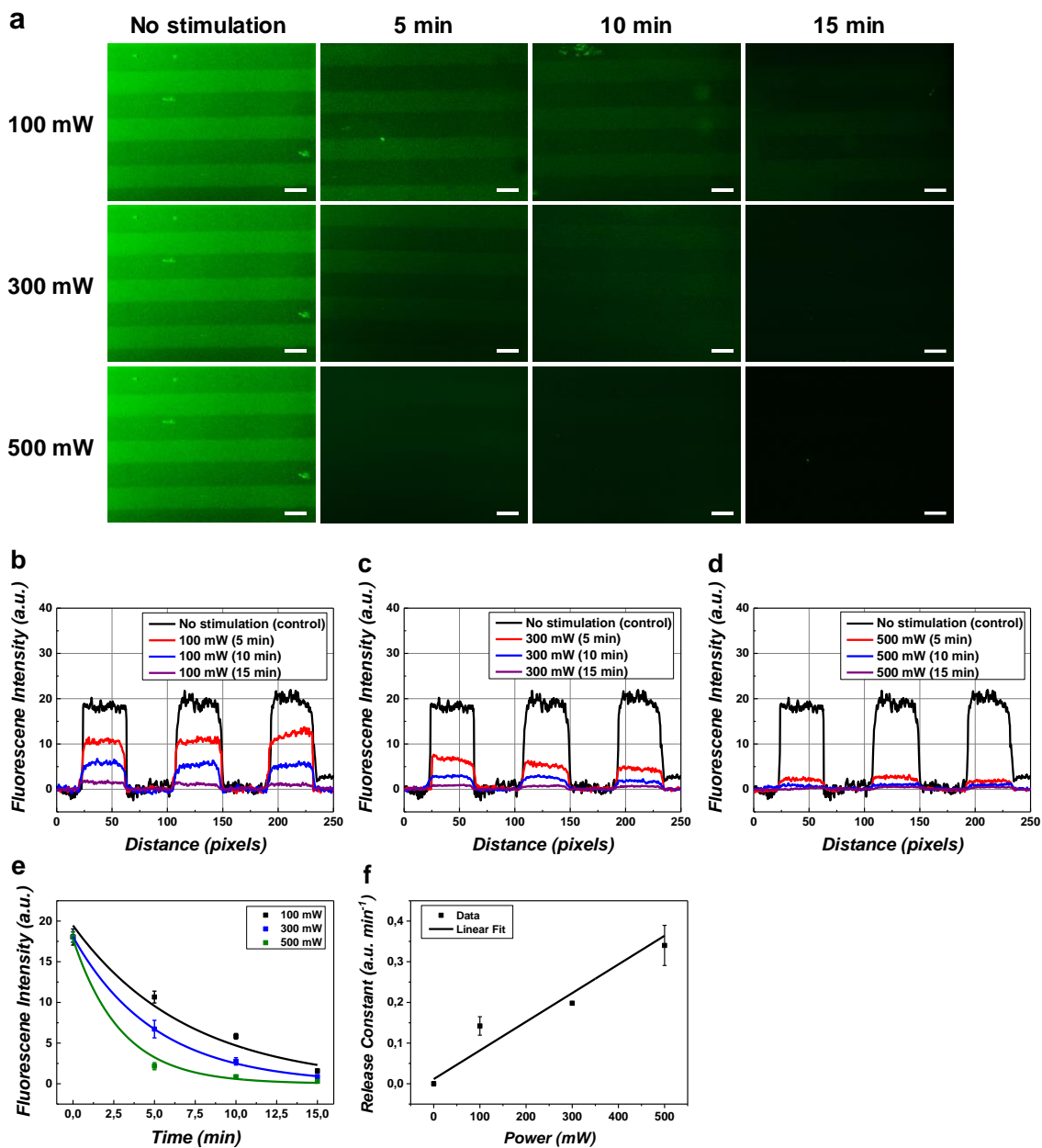
Figure S2. (a) Fluorescence imaging of line-patterned (by MIMIC), immobilized, CF-loaded (0.1 mM) PSVs before and after acoustic stimulation at different powers (100, 300 and 500 mW) and durations (5, 10 and 15 min). The scale bars are 10 μm. Changes of fluorescence intensity under acoustic stimulation at powers of (b) 100 mW (c) 300 mW and (d) 500 mW. (e) Fluorescence intensities of the released CF dye as a function of time at different powers, and exponential decay fits ($I = I_0 e^{-kt}$) of these curves. (f) Release rate constant k from the exponential decay fits of panel e as a function of power, and a linear fit to it.

For the *loading* of CF into PSVs in Figure 1b and Figure S1a, the fluorescence intensity of the pattered area stands for amount of the loaded CF inside the vesicles. Thus, the changes of fluorescence intensity at different powers that were extracted from Figure S1a can be used to measure the loaded CF per unit time, i.e. the loading kinetics. For the *release* of CF from PSVs as reported in Figure 1c and Figure S2a, the fluorescence intensity of the pattered area indicates the remaining CF dye after the release triggered by hypersound, which can be used to measure the release kinetics as shown in Figure S2d-e.

In Figure S3a-c, the released amount of CF dye from immobilized vesicles (now loaded from a 5 mM dye solution) was measured by using the fluorescence intensity of the solution in the sealed chamber, and the release kinetics at different powers is shown in Figure S3d and S3e. It should be noted, however, that the linear trends observed here are probably caused by relatively slow diffusion of the released dye into the bulk and the higher concentration of dye used to load the vesicles (needed because the low concentration used for Figure S2 was too low to observe release in solution), so that the solution signal is still increasing in time (Figure S3), while the surface data (Figures 1e and S2) indicate a faster depletion of the surface source. Most important, however, is that both measurement methods show a linear trend of release rate vs power.
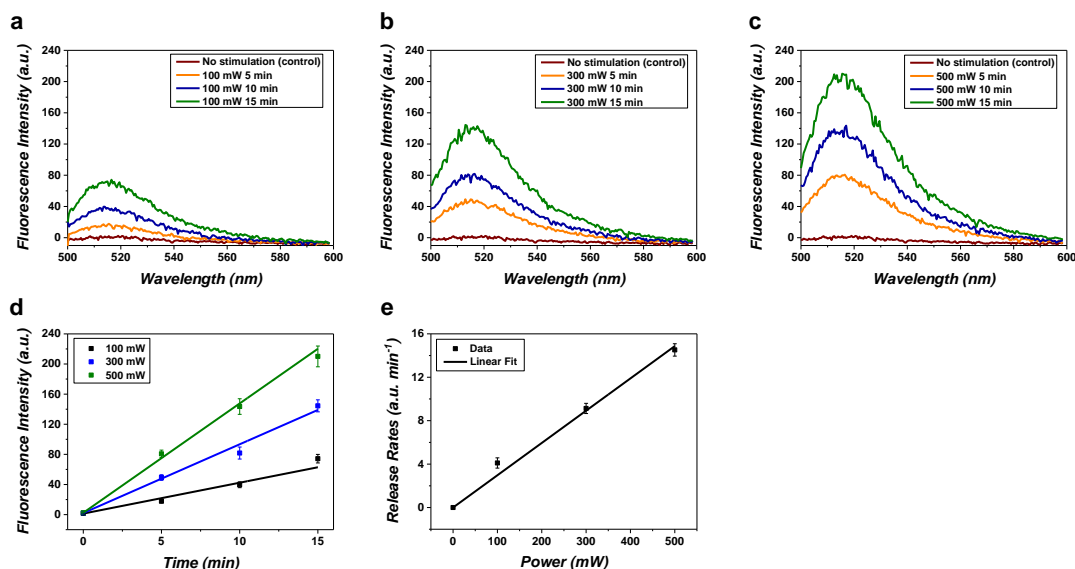
Figure S3. Fluorescence detection of the dye release from PSVs loaded with 5 mM CF immobilized on a surface. Fluorescence spectra of released CF triggered by acoustic stimulation at different powers of (a) 100, (b) 300 and (c) 500 mW. (d) Fluorescence intensity as a function of time, and linear fits (release rate) at different powers. (e) Release rate as a function of power.
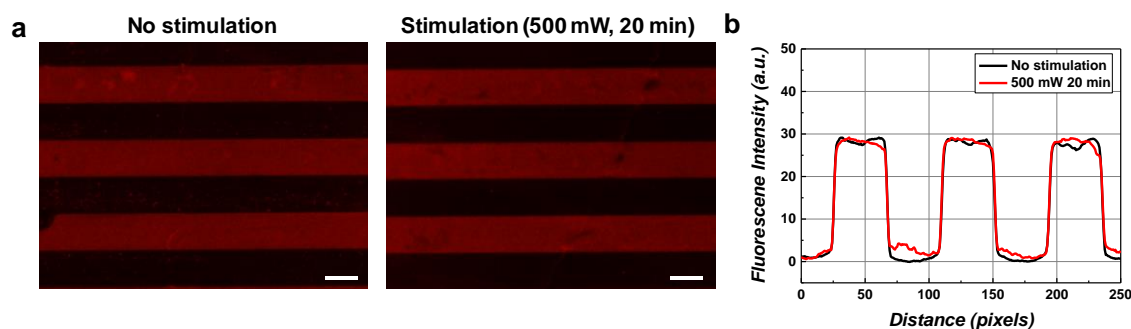
Figure S4. (a) Fluorescence microscopy images of rhodamine-B-labeled PSVs without and with acoustic stimulation (500 mW for 15 min). The scale bars indicate 10 μm. (b) Line profiles of fluorescence intensities extracted from immobilized PSVs.
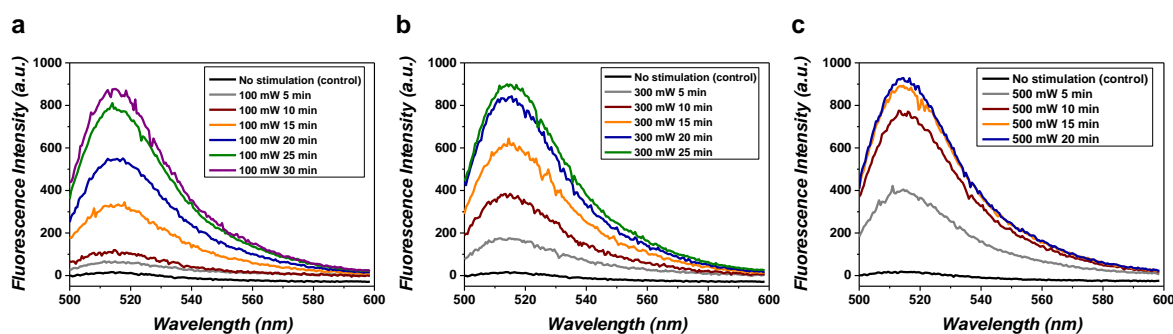
Figure S5. Fluorescence detection of controlled dye release from PSVs in solution. Fluorescence spectra of released CF dye triggered by acoustic stimulation at different powers of (a) 100 mW, (b) 300 mW, and (c) 500 mW, or without stimulation (control) as a function of time. In the control experiment, the fluorescence intensity of the solution in the upper chamber was detected after waiting for 20 min after dye-encapsulated PSVs were put in the lower chamber.
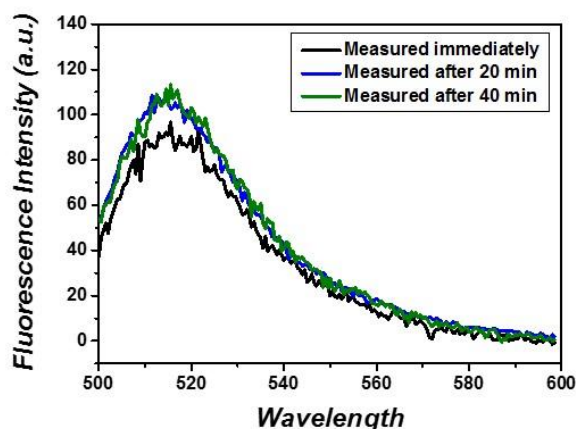
Figure S6. Fluorescence spectra of CF in the upper chamber measured immediately or upon waiting for 20 and 40 min after the acoustic stimulation was turned off.
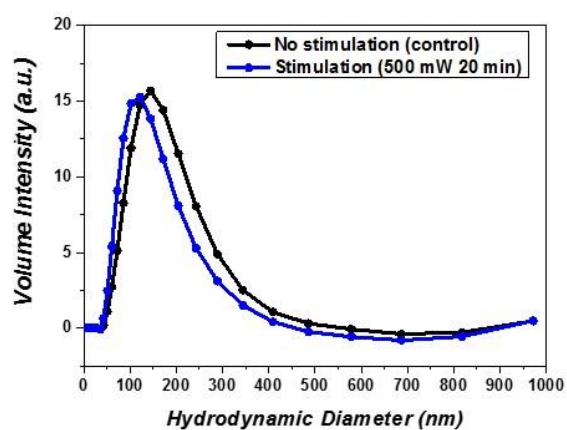
Figure S7. Size distributions by dynamic light scattering of PSVs before and after acoustic stimulation.

2. Deformation of individual GUVs

To study mechanical deformations of vesicles under acoustic streaming, GUVs were immobilized on a supported lipid bilayer (SLB) in a glass bottom 96-well plate (Figure S8). Both the GUVs and the SLBs were made from lipid mixtures of 1,2-dioleoyl-sn-glycero-3-phosphocholine (DOPC), Texas Red-functionalized 1,2-dihexadecanoyl-sn-glycero-3-phosphoethanolamine (Texas Red-DHPE), and 1,2-dipalmitoyl-sn-glycero-3-phosphoethanolamine-N-(cap biotinyl) (Biotin-cap-PE). After the deposition of the biotinylated SLB, we confirmed its mobility through fluorescence recovery after photobleaching (FRAP, Figure S9a). Thereafter, Alexa Fluor-488-labeled SAv was anchored onto the membrane surface, followed by the immobilization of biotinylated GUVs via biotin-SAv affinity pairs. Fig. S9b shows that the green fluorescence from SAv overlapped with the contact area of the vesicle, indicating that the specific biotin-SAv interaction pairs formed at the interface.
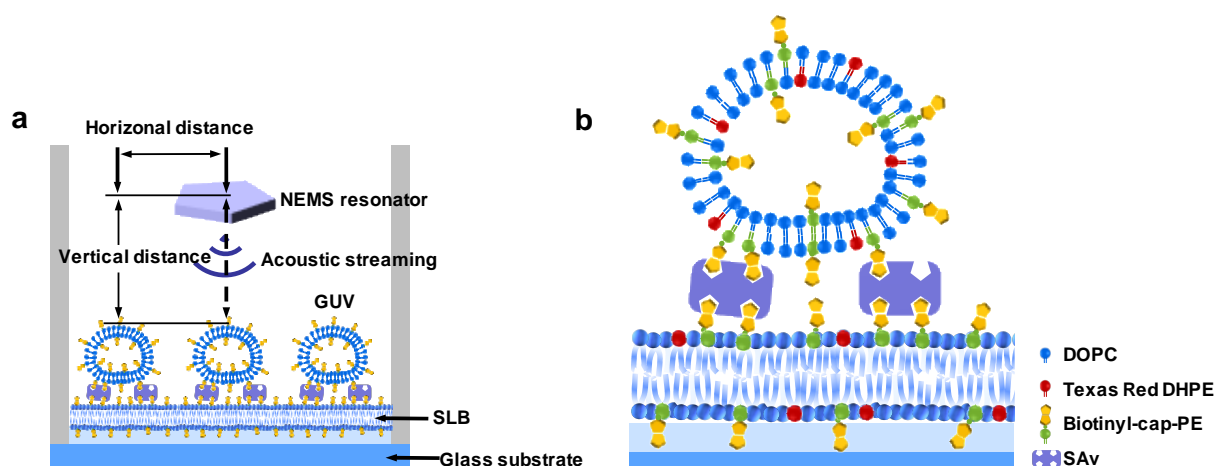
Figure S8. (a) System for the detection of mechanical deformation of immobilized GUVs. The acoustic resonator was mounted on a long rectangle-shaped evaluation board, which was inserted into the reservoir at variable depths. The distance between the immobilized GUV and the mounted resonator was controlled by the inserted position of the evaluation board. The GUV-SLB system was kept in sucrose buffer (100 mM, 20 mM Tris, pH 7.4) to keep the GUVs stable. (b) Schematic picture of the biotin-SAv binding motif used for the adhesion of GUVs to the SLB. Both the GUVs and the SLB are composed of DOPC, Texas Red-DHPE and Biotinyl Cap-PE.
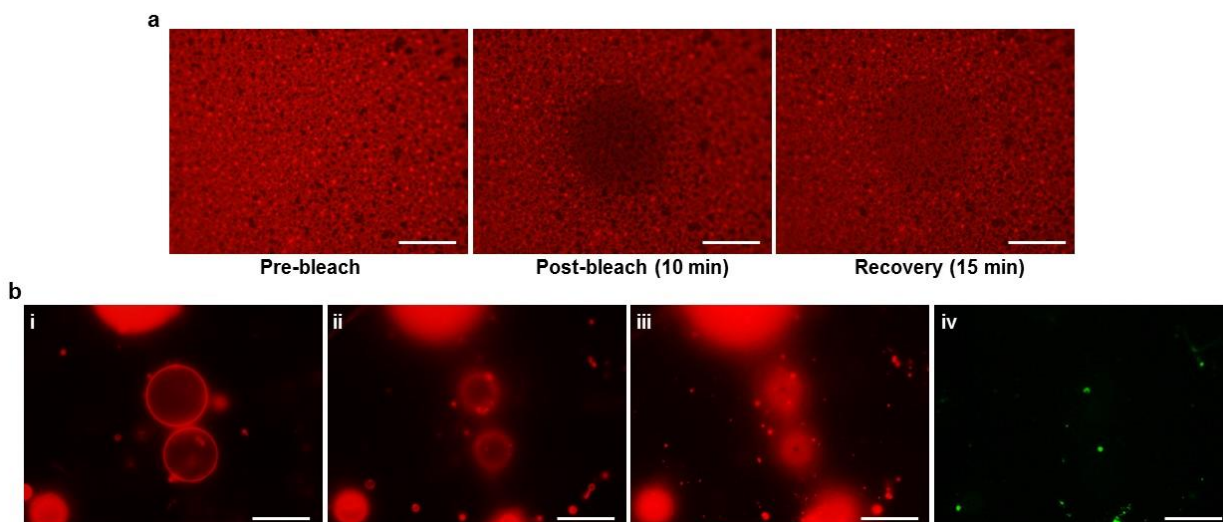
Figure S9. (a) Fluorescence images of the Texas Red-labeled SLB before bleaching (left), 10 min after exposure to a high-intensity laser with an excitation wavelength of 595 nm (middle), and 20 min after the excitation laser was shut off (right). (b) Fluorescence images of immobilized GUVs obtained at different focal planes. Images i to iii show the fluorescence of the Texas Red dye emitted by the GUVs. Image iv shows the fluorescence of the to the Alexa Fluor 488-labeled SAv. The adhesion of GUVs to the SLB was controlled by inter-membrane affinity pairs between SAv and biotin moieties on both GUV and SLB. The scale bars represent 20 µm.

The behavior of a GUV was recorded, using confocal laser scanning microscopy (CLSM, Figure S10a, Video S1-S4), under acoustic streaming at various powers, while the resonator was placed at a fixed distance of 100 µm from the surface. The vesicle showed a clear deformation under the acoustic streaming but recovered its initial shape instantly once the power was turned off. To quantitatively analyze the deformation in time, the aspect ratio (marked in Figure S10a) of the single GUV at each frame (Video S1-S4) was extracted by a custom written Matlab script and plotted for each power. These results show that, once the acoustic streaming was applied, the aspect ratio of vesicle increased immediately and remained at a fixed value until the stimulation was turned off. This behavior clearly indicates that acoustic streaming induces an instant and reversible deformation of vesicles. By increasing the supplied power, the acoustic response led to a correspondingly increased deformation.
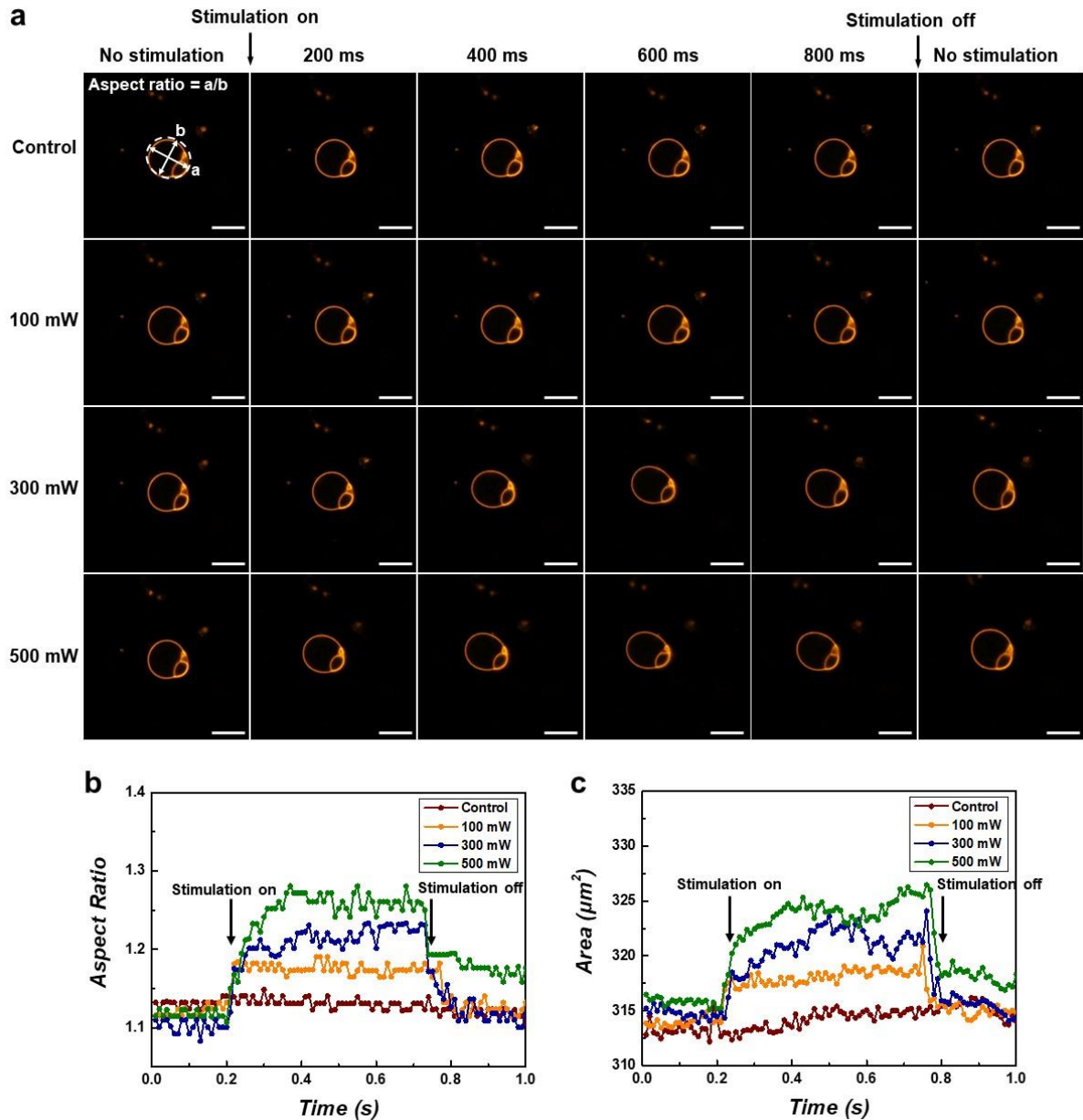
Figure S10. (a) Time sequences of CLSM images showing the deformation of a GUV upon stimulation by acoustic streaming at different powers (0, 100, 300 and 500 mW, extracted from Video S1-S4). The distance between the GUV and the resonator was fixed at 100 µm. The scale bars indicate 10 µm. We define the aspect ratio (referred to as *a/b* in (a)) of a single GUV to quantify its deformation. The outline (dashed line in (a)) was extracted by a custom written Matlab script, where *a* and *b* represent the long and short axes of the vesicle, respectively, and the value of *a/b* represents the aspect ratio of the vesicle in the projected area. Changes of the (b) aspect ratio and (c) projected area of the GUV as a function of time at various powers (100, 300, 500 mW) applied at a fixed distance (100 μm).

To evaluate its dependence on the vertical distance (marked in Figure S8a), the deformation of a GUV was monitored under acoustic streaming of the same power (300 mW) but at different distances from the resonator (Figure S11, Video S5-S8). It shows that the

vesicle deforms most strongly at 100 µm but less at lower or higher distances. This dependence can be attributed to the spatial distribution of the acoustic streaming, in which the streaming velocity starts to increase from the surface of the resonator and reaches its maximum value at a position with only tangential forces then gradually decreases with distance.
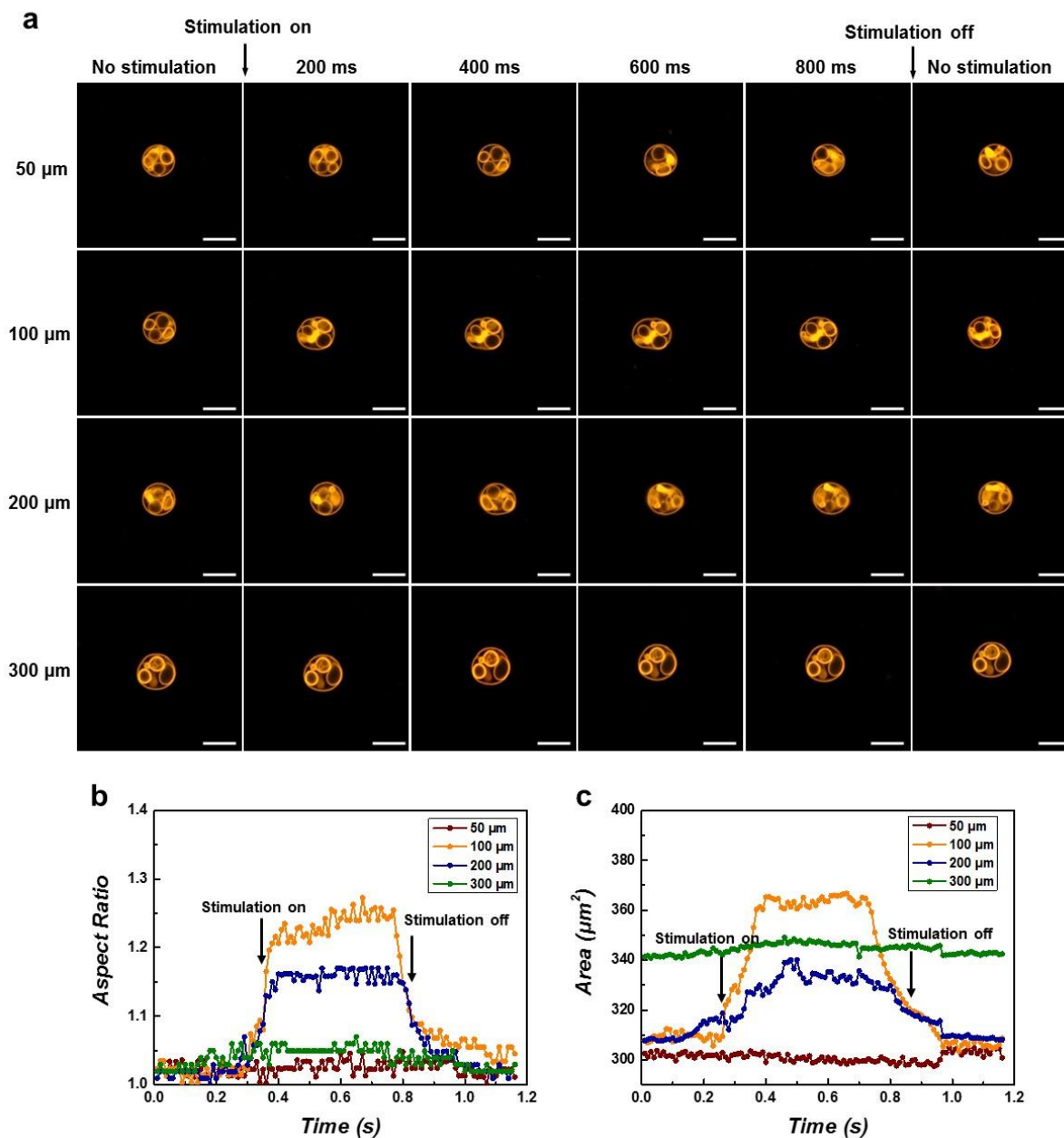
Figure S11. (a) Time sequence of CLSM images showing the deformation of a GUV with the same acoustic pressure at different distances (50, 100, 200 and 300 µm, extracted from Video S5-S8). The power of the GHz acoustic streaming was fixed at 300 mW. The scale bars indicate 10 µm. Corresponding changes of the (b) aspect ratio and (c) projected area of the GUV upon acoustic stimulation (300 mW).

Notably, at 500 mW, the aspect ratio of the GUV in Figure S10a did not completely recover to its original value upon turning off the stimulation. To further study this irreversible deformation, we applied 500 mW continuously to two adjacent GUVs for 800 ms (Figure S12a).

The relative distance between the two vesicles was reduced during the acoustic streaming and did not revert upon switching off. Compared to the original state, the contact areas of the two vesicles had also significantly increased (Figure S12b), which is likely due to enhanced compression of the vesicles at the SLB induced by the high-speed acoustic streaming. This assumption was confirmed by the 3D reconstruction of the GUV from the confocal z-stacks (Figure S12c), which shows that the height of the GUV decreased upon the stimulation at 500 mW for 800 ms. These results suggest that the contact area between the GUV and the SLB increases during the acoustically induced deformation at high power, which may increase the number of binding sites of the GUV with the anchored SAv on the SLB and cause an enlarged contact area of the GUV to the interface of SLB. With this higher number of interactions, the deformed GUV cannot fully recover to its original shape. Additionally, the acoustic streaming likely induced strong shear stresses at the vesicle surface, which in turn deform the vesicle.
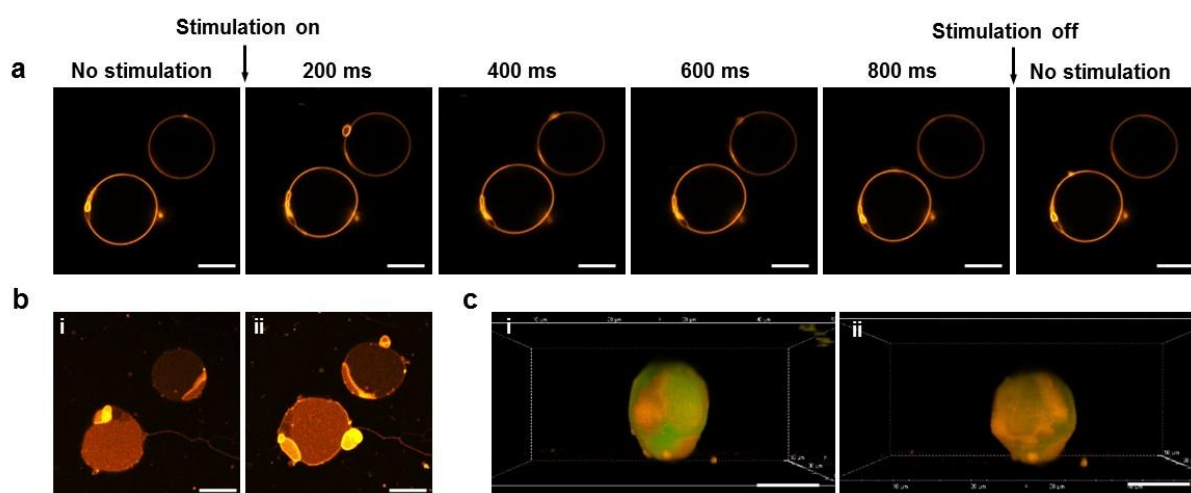
Figure S12. (a) Time sequence of CLSM images showing the deformation of two adjacent GUVs stimulated by acoustic streaming at 500 mW for 600 ms. The distance between the two GUVs and the resonator was fixed at 100 µm. (b) The binding areas between the GUVs and the SLB before (i) and after (ii) the acoustic stimulation (500 mW, 800 ms). (c) 3D reconstructions of an immobilized GUV before (i) and after (ii) the acoustic stimulation (500 mW, 800 ms). The scale bars indicate 10 µm.

The deformation experiment was also performed using a GUV loaded with Fluo-4 dye. As shown in Figure S13a, The green fluorescence emitted from Fluo-4 was clearly defined within the GUV during its deformation induced by the acoustic streaming (300 mW), confirming the integrity of the immobilized GUV under acoustic stimulation. The similar change of aspect ratio in Figure S13b verifies the reliability of this acoustic-induced deformation.
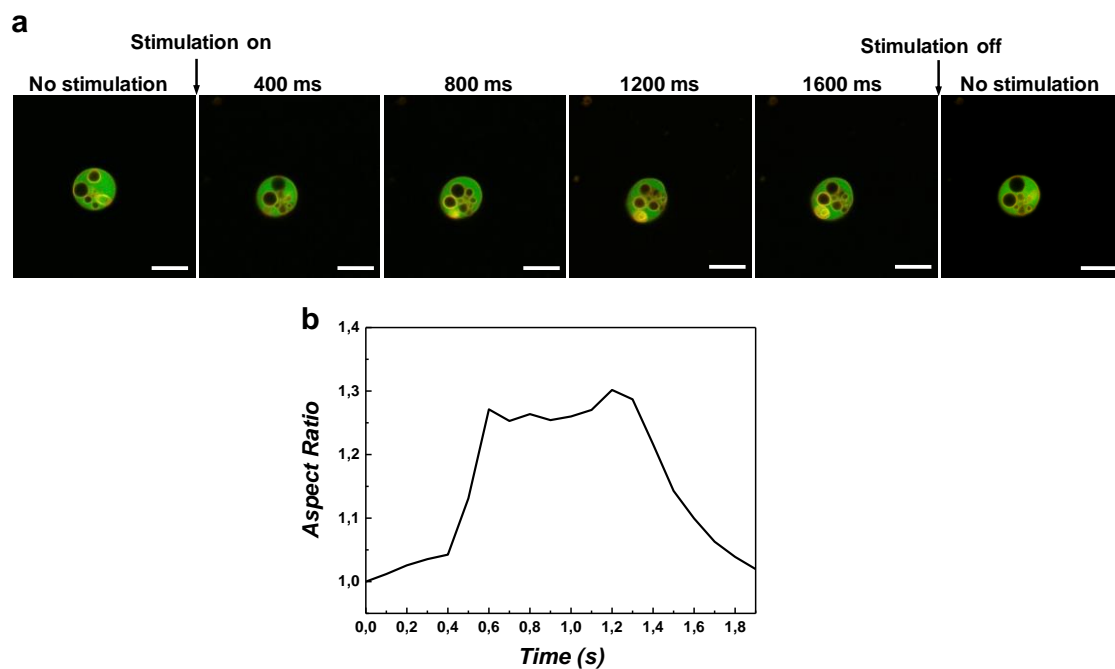
Figure S13. (a) CLSM images showing the deformation of a GUV loaded with Fluo-4 dye stimulated by acoustic streaming (300 mW). The distance between the GUV and the device was fixed at 100 μm. The scale bars indicate 10 μm. (b) Aspect ratio of the GUV as a function of time.

3. Investigation of the pore size by loading PS NPs into GUVs

To evaluate the size of the pores formed by acoustic streaming, we performed similar experiments with PS NPs of 100 and 200 nm. The orange fluorescence of 100 nm PS NPs was also observed inside the GUVs, but at a lower intensity; with red-fluorescent 200 nm PS NPs, however, their fluorescence was found only around and not inside the GUVs. This indicates that pores formed by the acoustic streaming at 300 mW are not sufficiently large and/or do not exist for a sufficiently long time to allow the transport of 200 nm NPs across the membrane. When the power of the acoustic streaming was increased to 500 mW, both the blue (50 nm PS NPs) and the orange fluorescence (100 nm PS NPs) intensities increased, while the 200 nm PS NPs still stayed outside the vesicle (Figure S14). This increase of intensity reveals that the loading of nanoparticles is power dependent, which we assume is related to the dynamic pore formation process generated during the deformation of vesicles. The reproducibility of this loading experiment is given by additional images of NP-loaded vesicles in Figure S15 by loading PS NPs of 50 nm into GUVs with acoustic streaming of 100 or 300 mW.

Note that in the case of 200 nm PS NPs, some particles remained visible on the outside even after rinsing with buffer solution for three times. However, in the case of 50/100 nm PS NPs, after they were loaded inside the vesicles, the fluorescence intensity became concentrated inside and much higher than the fluorescence from the remaining nanoparticles outside the vesicles. This contrast difference explains the apparent difference in background.
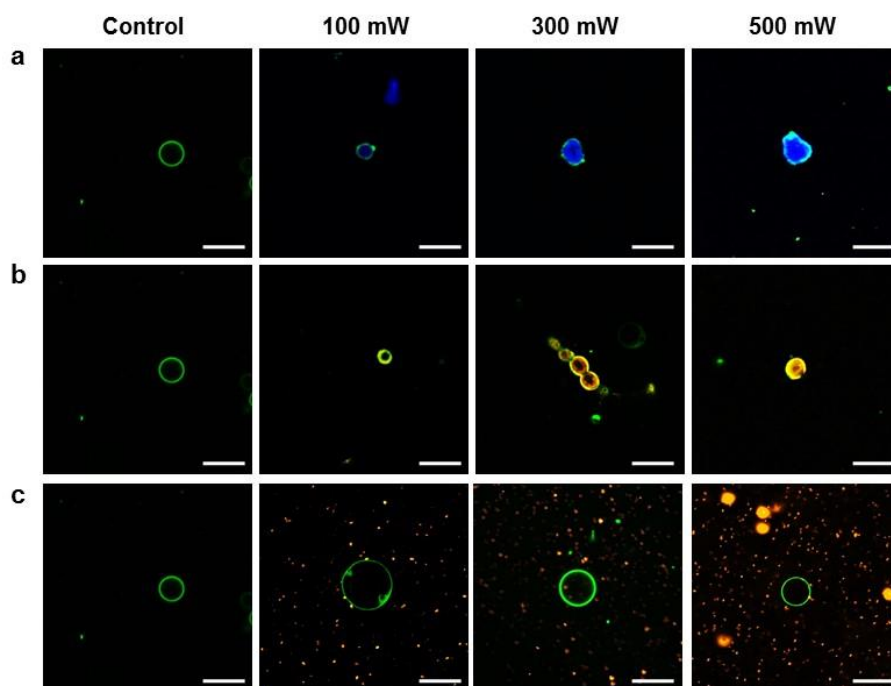
Figure S14. CLSM images of Top Fluor-labeled GUVs encapsulated with PS NPs of (a) 50 nm (blue fluorescence), (b) 100 nm (orange fluorescence) and (c) 200 nm (red fluorescence) without (control) or with (100, 300, 500 mW) acoustic stimulation at a fixed distance of 100 μm for 10 min. The scale bars indicate 10 μm.
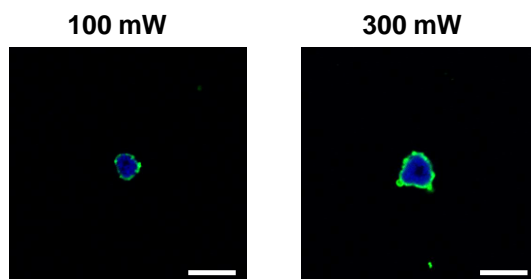
Figure S15. Additional images of loading experiments by PS NPs of 50 nm in the case of 100 or 300 mW acoustic stimulation. The scale bars indicate 10 μm.

4. Simulations of the GUV deformation

Figure 4a shows the simulated patterns of the acoustic streaming, where multiple micro-vortices can be seen around the resonator. The zoom-in image illustrates the hydrodynamics of the acoustic streaming around the vesicle and its displacement under these flow conditions.

Since the acoustic streaming can be tuned by the power applied to the resonator and the vertical distance from the bottom surface of the resonator, we further simulated the power and the distance dependencies. The field of the acoustic streaming around the vesicle was calculated and the hydrodynamic traction over the surface of the vesicle was integrated

to obtain the shear stress exerted on its surface (Table S1). As shown in Figure 4b, the total shear stress on the surface of the vesicle is proportional to the applied power, while it is not linearly proportional to the distance. For vesicles that were treated under the same power but at different distances, the shear stress reached a maximum value at ~100 μm and decreased at lower or higher distances. The occurrence of a maximum can be explained by the fact that the speed of the vortices decreases when extending their distance to the resonator, and that a minimum distance is required to get sufficient vortex speed. Moreover, the non-uniformly distributed acoustic streaming around the vesicle, which is related to the frequency, size, shape of the resonator and the relative position of the vesicle to the resonator, also plays a role. All these parameters determine simultaneously the optimal distance between the vesicle and the resonator to achieve the desired vesicle deformation.

To quantitatively evaluate the deformation of a spherical vesicle under different shear stresses, we simulated the deformation of the vesicle in response to the power and distance. As shown in Figure 4c, the aspect ratio of the vesicle increases upon the stimulation by the acoustic streaming, along which the corresponding projected area also extends (Figure S14b). Like the stress simulated above, the aspect ratio is proportional to the applied power but not directly proportional to the distance. The maximum deformation of the vesicle, i.e., the largest aspect ratio (1.56), appears at 100 μm and a power of 500 mW.

Table S1. Shear stresses on the surface of a GUV induced by acoustic streaming stimulated at different powers (100, 300 and 500 mW) at different distances (50, 100, 200 and 300 μm) to the resonator.

Distance (μm)	Power (mW)	Shear stress on GUV (pN)
50	100	0.226
50	300	0.818
50	500	1.590
100	100	0.380
100	300	1.260
100	500	2.320
200	100	0.243
200	300	0.739
200	500	1.250
300	100	0.138
300	300	0.411
300	500	0.679
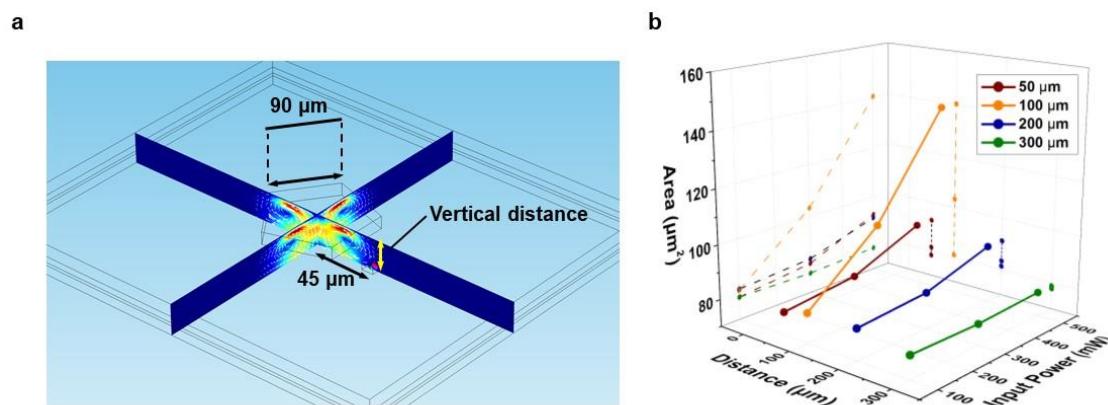
Figure S16. (a) Schematic of the 3D FEM simulation. The side length of the pentagonal resonator is 90 µm. In this model, a 10-µm vesicle was located at coordinates of (45 µm, 0 µm, -50 µm). The *x* value stands for the horizontal distance of vesicle from the center of the resonator while the *z* value stands for the vertical distance of the vesicle from the center of the resonator. The elastic properties of the vesicle shell were decided by fitting the first experimental data in Figure S10, based on which the Young's and shear modulus were automatically set in the software. (b) Mechanical deformations of the simulated vesicle in terms of the project area of the vesicle at different situations.

Supplementary videos

Videos corresponding to Figure S10.
Video S1. Control: Immobilized vesicles without any stimulation of hypersound.
Video S2. Deformation of vesicles under hypersound of 100 mW from a distance of 100 µm.
Video S3. Deformation of vesicles under hypersound of 300 mW from a distance of 100 µm.
Video S4. Deformation of vesicles under hypersound of 500 mW from a distance of 100 µm.

Videos corresponding to Figure S11.
Video S5. Deformation of vesicles under hypersound of 300 mW from a distance of 50 µm.
Video S6. Deformation of vesicles under hypersound of 300 mW from a distance of 100 µm.
Video S7. Deformation of vesicles under hypersound of 300 mW from a distance of 200 µm.
Video S8. Deformation of vesicles under hypersound of 300 mW from a distance of 300 µm.

References

1.   Samanta A, Tesch M, Keller U, Klingauf Jr, Studer A, Ravoo BJ. Fabrication of Hydrophilic Polymer Nanocontainers by Use of Supramolecular Templates. *J. Am. Chem. Soc.* **137**, 1967-1971 (2015).

2.   Falvey P, Lim CW, Darcy R, Revermann T, Karst U, Giesbers M, *et al.* Bilayer vesicles of amphiphilic cyclodextrins: host membranes that recognize guest molecules. *Chem.-Eur. J.* **11**, 1171-1180 (2005).

3.	Voskuhl J, Fenske T, Stuart MC, Wibbeling B, Schmuck C, Ravoo BJ. Molecular recognition of vesicles: host–guest interactions combined with specific dimerization of zwitterions. *Chem.-Eur. J.* **16**, 8300-8306 (2010).

4.	de Vries WC, Tesch M, Studer A, Ravoo BJ. Molecular Recognition and Immobilization of Ligand-Conjugated Redox-Responsive Polymer Nanocontainers. *ACS appl. mater. inter.* **9**, 41760-41766 (2017).